IGNITION AND SUBSEQUENT FLAME SPREAD OVER A THIN CELLULOSIC MATERIAL

by

Kazuyoshi Nakabe
Guest Researcher
Osaka University
Osaka, Japan
and
Howard R. Baum, and Takashi Kashiwagi
Building and Fire Research Laboratory
National Institute of Standards and Technology
Gaithersburg, MD 20899

National Aeronautics and Space Administration. 2nd International Microgravity Combustion Workshop, September **15-17, 1992,** Cleveland, Ohio. **167-179** pp. NASA **Lewis** Research Center, Cleveland, ON. 1992.

IGNITION AND SUBSEQUENT FLAME SPREAD OVER A THIN CELLULOSIC MATERIAL

Kazuyoshi Nakabe*, Howard R. Baum and Takashi Kashiwagi
Building and Fire Research Laboratory
National Institute of Standards and Technology
Gaithersburg, Maryland 20899

(Starting date of this project: February 1988)

Introdudion

Both ignition and flame spread on solid fuels are processes that not only are of considerable scientific interest but that also have important fire safety applications. Both types of processes, ignition and flame spread, are complicated by strong coupling between chemical reactions and transport processes, not only in the gas phase but also in the condensed phase. In most previous studies, ignition and flame spread were studied separately with the result that there has been little understanding of the transition from ignition to flame spread. In fire safety applications this transition is crucial to determine whether a fire will be limited to a localized, temporary bum or will transition into a growth mode with a potential to become a large fire. In order to understand this transition, the transient mechanisms of ignition and subsequent flame spread must be studied. However, there have been no definitive experimental or modeling studies, because of the complexity of the flow motion generated by buoyancy near the heated sample surface. One must solve the full Navier-Stokes equations over an extended region to represent accurately the highly unstable buoyant plume and entrainment of surrounding gas from far away. In order to avoid the complicated nature of the starting plume problem under normal gravity, previous detailed radiative ignition models were assumed to be one-dimensional (ref.1) or were applied at a stagnation point (ref.2). Thus, these models cannot be extended to include the transition to flame spread. The mismatch between experimental and calculated geometries means that theories cannot be compared directly with experimental results in normal gravity.

To overcome the above difficulty, theoretical results obtained without buoyancy can be directly compared with experimental data measured in a microgravity environment. Thus, the objective of this study is to develop a theoretical model for ignition and the transition to flame spread and to make predictions using the thermal and chemical characteristics of a cellulosic material which are measured in normal gravity. The model should take advantage of the microgravity environment as much as possible in the gas phase instead of modifying a conventional normal-gravity approach. A thermally-thin cellulosic sheet is considered as the sample fuel, which might ignite and exhibit significant flame spread during test times available in NASA's drop towers or in the space shuttle, without requiring a pilot flame. This last situation eliminates many complicating parameters such as pilot flame location, temperature, and size (ref.3).

---

* Guest researcher from Osaka University, Osaka Japan.

2. Theoretical Model

2.1 Gas Phase Model

The absence of gravity (microgravity is approximated to be zero gravity) removes the buoyancy-induced vorticity generation mechanism. The small scale of the planned experiment, together with the slow external flow (less than 10 cm/s), simulating the ventilation flow level in a spacecraft, implies a low Reynolds number flow domain. When surface pyrolysis is present, the thermally-induced surface blowing velocity must be taken into account, even at low Reynolds numbers. Both these concepts can be accommodated by assuming the velocity field to be a potential flow. The only loss is the no-slip boundary condition which is already relaxed in the classical Oseen approximation to low Reynolds number phenomena. This approximation is adopted and is implicit in the analysis. The conservation equations of mass, energy and species in the gas phase under low Mach number combustion and heat transfer conditions can be written as:

$$\frac{D\rho}{Dt}+\rho\nabla\cdot\vec{v}=0\ ,\quad \rho\frac{D\int_0^T c_p dT}{Dt}-\nabla\cdot(k\nabla T)=\Delta H\dot{m}_f+\dot{q}_R \tag{1}$$

$$\rho\frac{DY_{ox}}{Dt}-\nabla\cdot(\rho D\nabla Y_{ox})=-\nu\dot{m}_f\ ,\quad \rho\frac{DY_f}{Dt}-\nabla\cdot(\rho D\nabla Y_f)=-\dot{m}_f$$

We assume that the reaction is represented by a global one step Arrhenius reaction and its kinetic constants are selected. Equations (1) are supplemented by an equation of state, taken in a form appropriate for low-Mach-number flows. Now multiply the first of Eqs. (1) by enthalpy, h, and add it to the second. The result is:

$$\rho_\infty h_\infty\nabla\cdot\vec{v}-\nabla\cdot(k\nabla T)=\Delta H\dot{m}_f+\dot{q}_R \tag{2}$$

Equation (2) is the fundamental equation for determining the velocity field $\vec{v}$. Since $\vec{v}$ is a vector field it can be decomposed into the gradient of a potential ϕ and a solenoidal field $\vec{u}$.

$$\vec{v}=\nabla\phi+\vec{u}\ ,\quad \nabla\cdot\vec{u}=0 \tag{3}$$

Substitution of Eq. (3) into Eq. (2) yields:

$$\nabla^2\phi=\frac{1}{\rho_\infty h_\infty}(\Delta H\dot{m}_f+\dot{q}_R+\nabla^2\psi)\ ,\quad \psi=\int_{T_\infty}^{T}k(T)\,dT \tag{4}$$

Note that the third term on the right hand side of the first equation of Eq. (4) can be eliminated by introducing a particular solution ϕ_P as:

$$\phi_P=\frac{\psi}{\rho_\infty h_\infty} \tag{5}$$

Moreover, it is convenient to introduce another particular potential $\phi_{P\infty}$ representing the effects of the external wind velocity u_∞. Then, introducing a remainder potential Φ, ϕ may be expressed in the

$$\phi = \phi_P + \phi_{P_\infty} + \Phi \quad , \quad \nabla^2 \Phi = \frac{\Delta H \dot{m}_f + \dot{q}_R}{\rho_\infty h_\infty} \qquad (6)$$

mf

Equations *(5)* and (6) relate the potential field to the temperature distributions in the gas phase. In the calculation the sample is irradiated and auto-ignited at the center by continuous thermal radiant flux with a Gaussian distribution. Far from the surface, ϕ, T and Y_i must decay to their ambient initial values. T and Y_i decay exponentially to their ambient values. However, the potential field decays slowly away from the heated region. Thus, putting ϕ or its gradient equal to zero at the computational boundary would introduce unacceptable error into the calculation. These errors are avoided by using the analytical solution to Eq.(6) subject to the boundary condition at the sample surface to generate accurate values for ϕ on the computational boundary (ref.4). Then, Eqs.(1) are solved by a time-splitting algorithm.

2.2 Condensed Phase Model

It is assumed that the condensed phase is a thermally thin sheet of cellulosic material, and uniform in composition through its depth. The thermal degradation of the cellulosic sheet is described by two global thermal degradation reactions and a char oxidation reaction (ref.5). They are; (1) endothermic global pyrolysis reaction which degrades the cellulosic sheet to gases and a char, (2) weakly exothermic global thermal oxidative reaction which degrades the cellulose sheet to gases and a char, (3) highly exothermic global char oxidation reaction which degrades the char to gases and ash. Here, it is assumed that the reactivity of the chai with oxygen formed from the above two reactions with oxygen is the same. In the above global reactions combustible *gases* represent hydrocarbons and CO and non-combustible gases represent CO_2 and H_2O. Here, it is assumed that the combustible gases formed from each reaction above are the same. Although these reactions are crudely approximated compared to the actual, extremely complex degradation reactions, their accuracy is comparable to the global one-step gas phase oxidation reaction for the combustible gases, which is used for the gas phase reaction in this study.

The reaction rate of each reaction above, RR_i, is approximately expressed by the following Arrhenius-type equations:

$$(1)\ RR_p = A_p(\rho_s Y_f/\rho_{s0})^{np}\exp(-E_p/RT)$$
$$(2)\ RR_{ox} = A_{ox}(\rho Y_{ox}/\rho_{0,ox})^{nox}(\rho_s Y_f/\rho_{s0})^{nf,ox}\exp(-E_{ox}/RT)$$
$$(3)\ RR_{char} = A_{char}(\rho Y_{ox}/\rho_{0,char})^{no2,char}(\rho_s Y_{char}/\rho_{s0})^{nchar}\exp(-E_{char}/RT)$$

Values for the above kinetic parameters together with the heats of reaction, ΔH_i, for a black cellulosic paper have been measured; the details are given in Ref.5.

The equations for the condensed phase are given as follows.

Conservation of solid mass:

$$\partial(\rho_s/\rho_{s0})/\partial t = -(1 - \nu_{char,p})RR_p - (1 - \nu_{char,ox})RR_{ox} - (1 - \nu_{ash,char})RRchar \qquad (7)$$

Conservation of initial cellulosic material:

$$\partial(\rho_s Y_f/\rho_{s0})/\partial t = -RR_p - RR_{ox} \qquad (8)$$

Conservation of char:

$$\partial(\rho_s Y_c/\rho_{s0})/\partial t = \nu_{char,p}RR_p + \nu_{char,ox}RR_{ox} - RRchar \qquad (9)$$

Conservation of energy:

$$\delta\cdot\partial(\rho_s c_s T)/\partial t = (-\Delta H_p RR_p - \Delta H_{ox} RR_{ox} - \Delta H_{char} RR_{char})\cdot\rho_{s0}\delta + (1-r)\dot{q}_{ex} - \varepsilon\sigma(T_s^4 - T_0^4) + k\partial T(r,0,t)/\partial z \quad (10)$$

where δ is the half-thickness of the paper. The mass flux of evolved combustible gases from the surface is given by the following expression:

$$\dot{m}_s = [(1-\nu_{char,p})RR_p + (1-\nu_{char,ox})RR_{ox} + (1-\nu_{ash,char})RR_{char}]\rho_{s0}\delta \quad (11)$$

The cellulosic material used in the present study is a 0.38×10^{-4} m thick sheet.

3. Results and Discussion

Four different cases are being studied: (1) heat transfer with the degradation of the paper sheet irradiated by the external radiation at the center of the paper in an axisymmetric configuration, no gas phase reaction; no external flow, (2) ignition and subsequent flame spread in an axisymmetric configuration; no external flow, (3) heat transfer with a slow external flow in a three-dimensional configuration, and (4) ignition and subsequent flame spread with a slow external flow in a three-dimensional configuration. Since the results in the first case were published in ref.4, they are not discussed here due to space limitations.

3.1 Quiescent axisymmetric configuration

A maximum external radiant flux of 5 W/cm^2 (continuously on during computation) at 21%, 30% and 50% oxygen concentrations was used in the calculation. The results indicate that ignition is observed for 21% and 30% oxygen concentrations but the transition to flame spread does not occur. However, in 50% oxygen the transition is achieved as shown in Fig.1 which plots the gas phase temperature distribution at 1.0s after initiation of the external radiation. Each temperature isotherm line is a 100°K interval starting from 350°K. There are two high temperature regions;one is behind the flame front and the other is at the center where the external radiation continuously irradiates the sample. The results at later time show that there are two separate flames; the primary flame propagates radially outward, while the secondary flame stays at the center and becomes gradually weaker and disappears. Eventually one ring-like flame appears to continue its spread radially outward. The distribution of velocity vectors at the same time is shown in Figs.2. The large expansion flow motion near the flame front is clearly seen in Fig.2. The large mass addition near the center is caused by the continuously applied external radiation. Since the sample was nearly completely converted to char at the center, little mass is added there. The distribution of oxygen and fuei concentration indicates that the flame near the traveling front is a premixed flame followed by a diffusion flame behind the flame front. The energy balance at the sample surface at 1.0s is shown in Fig.3, where Q_{ex} is the external radiant flux, Q_{rad} is the re-radiation loss, Q_{rr} is the net heat balance of the three solid degradation reactions and Q_{conv} is the convective/conductive heat transfer from the gas phase to the sample. A high energy feedback rate of nearly 6 W/cm^2 is calculated as opposed to the nearly 1 W/cm^2 for the 21% oxygen concentration case at 1.6s after initiation of the external radiation as shown in Fig.4. This difference in energy feedback rate is mainly caused by differences in flame temperature (about 1400°K for 21% vs 2000°K for 50%) and also in the location of the peak gas phase reaction rate (closer to the sample surface in 50% oxygen concentration).

The previous experiment in a quiescent microgravity environment showed that the flame spread limit is about 20% oxygen for a light paper towel (Kimwipes paper) (ref.6). Thus, unsuccessful transition to flame spread in 21% and 30% oxygen predicted in this study does not agree with successful transition observed in the experimental work. Also, the predicted flame spread rate in 50% oxygen concentration is about 19 cm/s which is roughly five times faster than the experimentally-measured rate using the drop tower (ref.6). In the calculation the only uncertainty is the kinetic constants for the gas phase oxidation reaction. Since

there are no data available on the degradation products of the paper, the accuracy of the selected values is questionable. Since there are significant differences between the experimental setup and the calculation, for example, a two-dimensional experimental configuration vs. an axisymmetric calculation and piloted ignition in the experiment vs. auto-ignition, no attempt is made to adjust the kinetic constants of the gas phase reaction to match with the experimental data. These constants will be measured in the future.

3.2 Three-dimensional Calculation

Although preliminary results on ignition in the three dimensional configuration with a slow external flow have been obtained, more time is needed to determine their accuracy and correctness. It is hoped that the results will be presented at the meeting. Here, the results for the three dimensional heat transfer problem are briefly discussed. In this problem either a thermally thin or thick non-reactive condensed material is irradiated by continuously applied external radiation with a Gaussian flux distribution. Typical examples of the distributions of velocity vectors relative to the ambient flow and temperature contours in the gas phase for a thermally thick non-reactive material are shown in Figs. 5 at 8s after the initiation of an external radiant flux of 4 W/cm^2 with an external velocity of 2 cm/s (from left to right). The left corner figure in Figs. 5 represents the front view (looking in the downstream direction) distribution. The top rectangular figure represents the side view of the distribution and the lower rectangular figure represents the top view of the distribution. The distribution of velocity vectors represent the flow motion generated by heat addition from the irradiated surface. This flow is smaller than the external flow of 2 cm/s. Its center is located at a short distance upstream from the center of the external irradiation (x=0). This indicates that the steepest temperature gradient occurs at the upstream location due to downward pushing of the heated layer by the ambient flow. At a short distance downstream from x=0, there is a sink of flow due to the steep temperature gradient due to heat loss from the hot gas stream to the cold surface. Since the temperature gradient drives the flow, the flow generated by the external radiation is limited to a region near the irradiated surface area at an early time.

4. Future plans

1. Complete development of the three-dimensional ignition and flame spread code.
2. Conduct parametric study to determine which parameters affect ignition, the tmsition, and flame spread.
3. Measure global gas phase oxidation reaction rate for the degradation products of the paper.
4. Modify the codes to include piloted-ignition.

Reference

1. Kashiwagi,T, "A Radiative Ignition Model of a Solid Fuel", *Combustion Science and Technology, 8,* 1974, pp.225-236.
2. Amos,B. and Fernandez-Pello,A.C., "Model of the Ignition and Flame Development on a Vaporizing Combustible Surface in a Stagnation Point Flow: Ignition by Vapor Fuel Radiation Absorption", *Combustion Science and Technology, 62,* 1988, pp.331-343.
3. Tzeng,L.S., Atreya, A., and Wichman,I.S., "A One-Dimensional Mode! of Piloted Ignition", *Combustion and Flame, 80,* 1990, pp.94-107.
4. Kushida,G., Baum,H.R., Kashiwagi,T. and di Blasi, C., "Heat and Mass Transport from Thermally Degrading Thin Cellulosic Materials in a Microgravity Environment", *Journal* of Heat *Transfer,* 114, 1992, p.p484-502.
5. Kashiwagi,T. and Nambu,H., "Global Kinetic Constants for Thermal Oxidative Degradation of a Cellulosic Paper", *Combustion and* Flame, *88,* 1992, pp.345-368.
6. Olson,S.L., Ferkul,P.V., and Tien,J.S., "Near-Limit Flame Spread Over a Thin Solid Fuel in Microgravity", *Twenty Second Symposium (International) on Combustion,* The Combustion Institute, Pittsburgh, PA, 1988, pp.1213-1222.

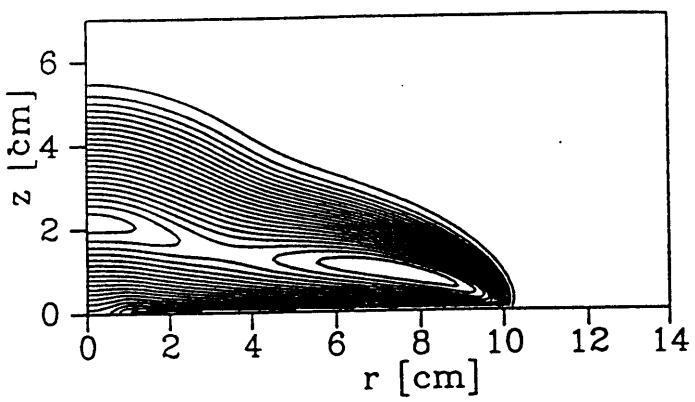

Fig. 1 Temperature contour in the gas phase

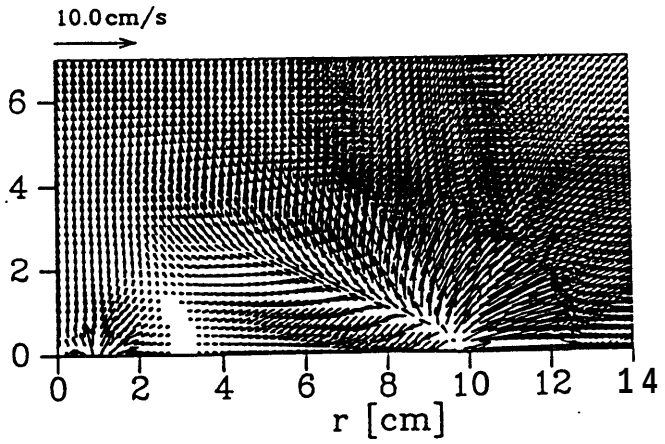

Fig. 2 Velocity vector

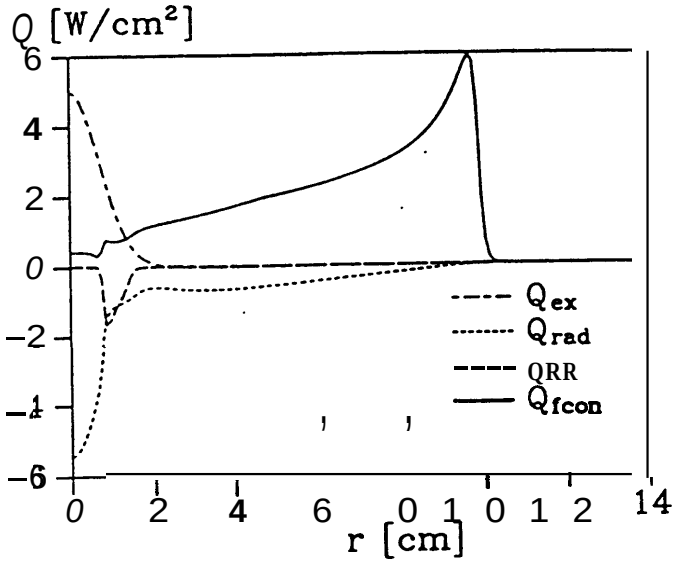

Fig. 3 Energy balance at the surface 50%oxygen

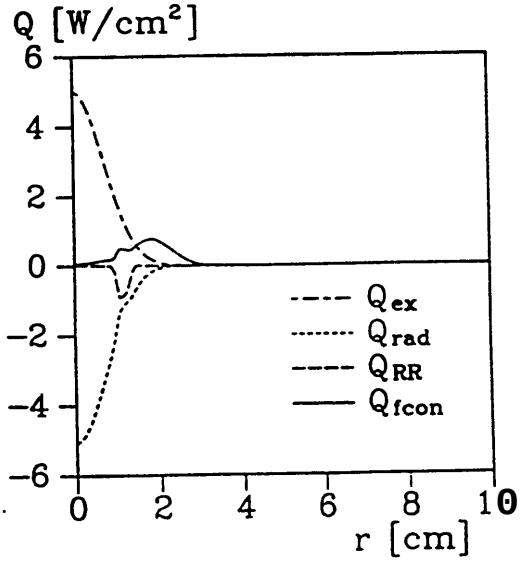

Fig. 4 Energy blanace at the surface in air

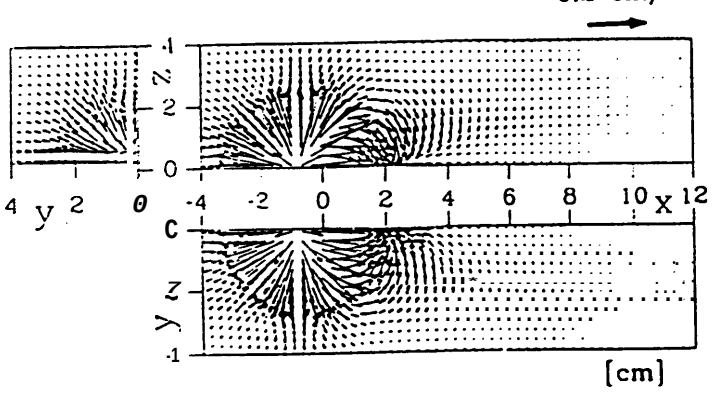

Fig. 5 Velocity vector in 3D flow

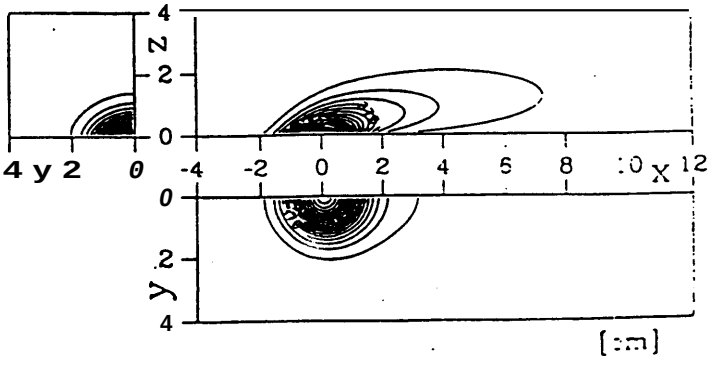

Temperature contour in 3D flow

COMBUSTION OF SOLID FUEL IN VERY LOW SPEED OXYGEN STREAMS
(NASA Grant NAG3-1046, Starting Date: May, 1989)

James S. T'ien*, Kurt R. Sacksteder†, Paul V. Ferkul', Gary D. Grayson*
* Case Western Reserve University
† NASA Lewis Research Center

1. Introduction

In reduced gravity, the combustion of solid fuel in low-speed flow can be studied. The flame behavior in this low-speed regime will fill a void in our understanding of the flow effect on combustion. In addition, it is important for spacecraft fire safety considerations. In this work, modeling and experimental work on low-speed forced-concurrent-flow flame spread are carried out. In addition, experiments on reduced-gravity buoyant-flow flame spread are performed.

2. Low Speed Forced Flow

2.1 Concurrent-Flow Flame Spread Model [1]

The model considers two-dimensional, steady flame spread in concurrent flow over a thin solid. Because of its thinness, the fuel bed can burn through. The flame could therefore reach a constant length provided that a constant (and equal) flame tip velocity, pyrolysis front velocity, and fuel burnout rate, can be obtained in the low-speed concurrent flow environment.

The flame is assumed to be laminar because of its small size and low velocity. The gas-phase fluid mechanical treatment is more comprehensive than most works in the past. In the flame base region (where the upstream flow is seen first), streamwise heat and mass diffusion is included. This, together with finite-rate, gas-phase chemical kinetics, enables us to examine the question of flame stabilization and extinction. The elliptic treatment of this flame stabilization zone entails the full Navier-Stokes equations. On the other hand, to save computational time, a boundary layer approximation is employed in the downstream region. The two zones are coupled at an appropriate gas-phase location. They are also coupled indirectly through the solid by energy exchange. A simplified solid fuel model is used. The solid is assumed to be thermally thin and to pyrolyze according to a one-step Arrhenius law with no char and tar formation. A solid-surface radiative-loss term is included which becomes critically important in the low-speed flammability limit. Because of the coupling between elliptic and parabolic regions and between the gas and solid phases, the numerical solutions require many iterations and are computationally intensive; they are carried out using the Cray X-MP Supercomputer at the NASA Lewis Research Center.

Although the model has been formulated for a mixed forced and buoyant flow, extensive computations have been performed for purely forced flow only, using oxygen mole fraction and free-stream velocity as parameters. Fig. 1 gives all the points calculated and the extinction boundary. Some of the important results are summarized below.

> The extinction boundary consists of a quenching and a blowoff branch similar to those in stagnation-point flow [2] and in opposed-flow flame spreading [3]. The quenching limit is due to the surface radiative loss. Without radiative loss, the model predicts no low-speed limit. Fig. 2 shows the maximum computed flame temperatures. In all cases, the maximum temperature decreases with flow velocity, especially near the quench limit. The flame spread rate decreases monotonically with flow velocity, as expected (Fig.3).
>
> Flames quench at low speed by shrinking in size. Near-limit flames remain stabilized in the fuel burnout region, as shown in Fig. 4. This fixed stabilization is in contrast to flame blowoff at higher

speed where the flame cannot be stabilized in the fuel burnout region. Extinction is reached when the flame is blown downstream. This illustrates one of the distinctions in flame extinguishment between quenching and blowoff. This difference becomes clear in a two-dimensional analysis but is obscure in one-dimensional sagnation-point flames. The reactivity contours shown in Fig. 4 resemble the visible blue flame seen in experiment (take $w=10^{-4}$ g/cm^3/sec for example), which will be discussed in the next section.

Using finite-rate kinetics enables us to examine the integrated flux of fuel vapor crossing any vertical plane. Far downstream, the fuel-flux stops changing (because the reaction becomes frozen), providing a measure of fuel escaping the flame. The fraction of fuel not consummed in the flame increases dramatically at lower speeds because of the increased importance of flame-tip quenching. Additionally, the variation of escaped fuel vapor is not monotonic with flow velocity.

22 Forced Concurrent Flow Flame Spread Experiments [4]

Low-speed concurrent-forced-flow experiments were conducted at Lewis Research Center's 5-second drop tower using thin tissue paper Kimwipe) as the solid fuel. The relative flow was generated using a sample translation device in a total of twenty-seven drop tests. In these tests, the flow velocity was varied from less than 1 cm/s to 5 cm/s and the oxygen concentration in nitrogen (at normal atmospheric pressure) from 30% down to extinction. Color cine films were made of the flames.

While in most tests the leading edge of the fuel receded steadily as it was burnt following the ignition transient, the downstream flame tip propagation was unsteady. Flames grew in length (after the ignition transient) at higher oxygen concentrations and relative flow velocities, but shrunk at lower concentrations and velocities. In higher-speed flows, in normal gravity, flame length has always been observed to grow after ignition [5]. The shrinking flames observed in these microgravity tests could be quenching, but the slow evolution of the flame length in the 5 second test time did not allow enough time to observe their eventual fate. Alternatively, the small, slowly evolving flames may be indicative of neat-steady configurations of flames in very-low-speed concurrent flows. Fig. 6 (the color photos are grouped together) shows a comparison of flames at approximately 5 cm/sec relative concurrent flow at three different oxygen concentrations. The shape of the 15% oxygen concentration case can also be compared favorably with the computed reaction contours (e.g. 10^{-4} g/cm^3/sec) shown in Fig. 4 for the same test condition.

The measured spread rates of the flame base, the leading edge of the fuel at which burnout occurs, are similar to the computed values shown in Fig. 3. However, spread rates at high oxygen concentrations and high relative-flow velocities are lower experimentally at the end of the drop while the rates at low oxygen concentrations and low relative-flow velocities are higher experimentally. These observations are consistent with the suggestion that the flames might not have had sufficient time to reach their final configuration in the available 5 seconds.

A flammability map, based upon the status of flames at the end of 5 seconds of microgravity, has been drawn and is similar to Fig. 1. No detailed comparison can be made because steady flames have not been achieved experimentally. It is clear that even for a thin fuel such as Kimwipes, which provide ample steady flamespread data in opposed-flow configurations, longer microgravity duration is needed to satisfactorily determine flame spread rates and extinction limits in concurrent flow.

3. Buoyant-Flow Flame Spread in Reduced-Gravity Experiments

Flame spread in buoyant flow under reduced-gravitational conditions has been observed using the NASA KC-135 aircraft flying parabolic trajectories at approximately 1/3rd, 1/6th, and 1/10th normal earth gravity levels. The test apparatus includes provisions for controlled ignition energy, color-schlieren flame imaging and three dimensional measurements of the local acceleration levels. Tests were conducted in O_2/N_2 mixtures from 18% oxygen down to extinction (of the same thin Kimwipe tissues used in our other tests) at normal and reduced pressures for upward (concurrent flow) flame propagation: and at normal pressure for downward (opposed flow) propagation.

3.1 Downward Flame Spread and Extinction

Schlieren images of flames spreading in buoyant, opposed flow showed steady propagation in oxygen concentrations below the normal-gravity flammability limit. At each oxygen concentration (18, 16, and 15% oxygen) spread rates decrease with increasing acceleration, though the difference between 1/10th g and 1/6th g is small. Tests conducted at 14% oxygen showed flame propagation at 1/10th g, and a blowoff extinction was observed during the aircraft pullout maneuver to approximately 2g. Flames at higher acceleration levels and 14% oxygen did not appear to survive the ignition transient. Fig. 5 shows a flammability map using acceleration level and normal-atmospheric-pressure oxygen concentration as parameters. The solid line gives the high-g blowoff boundary. The low-g extinction boundary, which cannot be determined accurately in the aircraft experiment, is indicated by the shaded curve. Fig. 7 shows schlieren images of the downward spreading flames at 15% oxygen at two reduced-gravity levels.

3.2 Upward Flame Spread

Schlieren images of flames spreading in buoyant, concurrent flows show propagation of flames down to normal-atmospheric-pressure oxygen concentrations of 12%, in both 1/6th and 1/3rd g. A single test at 1/10th g did not result in a propagating flame at 12% oxygen, while another at 14% did.

At normal atmospheric pressure, the upward spreading flames were characterized by thermal/flame plumes that become unsteady downstream of the flame stabilization zone. The tissue-paper fuel tended to curl, particularly in the normal pressure tests, disturbing the bottom of the flame. Fig. 8 a and b show two parts of an upward propagating flame at 15% oxygen in 1/6th g as they passed by the single schlieren window. In Fig. 8a, the unsteady/unstable plume is shown, while in Fig. 8b, the bottom of the flame is shown stabilized near the lowest point on the fuel surface.

Tests were conducted at reduced pressure and showed the existence of low-pressure limits. In the small number of tests conducted, the pressure limits were not determined with precision. At reduced pressure the flame plumes were more laminar and the fuel deformed more slowly during burning. Fig. 8c shows the downstream plume of a 15% oxygen, 0.5 atmosphere pressure flame at 1/6th g. Below, in Fig. 8d, the stabili d bottom of the same flame is shown.

4. Future Plans

Although surface radiative loss is included in the current model and has proven to be important in low-speed flows, gaseous radiation has been neglected. In stagnation point flow, gas radiation is found *to* alter the low-speed quenching limit for one-dimensional stationary flames. In concurrent flow gaseous radiation is likely to be more important because the flame is longer. Comparison with experiment also shows that without gas radiation the model overpredicts the flame length. The inclusion of gaseous radiation in the model is the logical next step and will complete our understanding of radiative effects on flame spreading over solid fuels in low speed flows. At the Same time thermally-thick solid fuel needs to be treated in the theory (presently, we have dealt with thermally-thin fuel only). The new elements that need *to* be added will include solid-phase heat transfer, fuel geometry change and an unsteady flame growth process.

Experimentally we will also begin *to* test thicker fuels in low-speed flows. Because of the limitations of microgravity time in ground-based facilities, steady state is not expected, even were burnout possible. In order for the results to be useful, a controlled ignition process will be extended *to* thick fuels. The ignition transient experiments and related modeling will lead to a rational design of a space-based experiment required to obtain concurrent-flow flame spreading data in the very low-speed regime.

Because of the flammability limit data we have obtained for both low-speed forced flow and buoyant flow in reduced gravity, we also hope to contribute to the reevaluation of flammmability test methods for spacecraft materials.

REFERENCES

1. Ferkul, P. V.: A Model of Low-Speed Concurrent-Flow Flame Spread over a Thin Solid Fuel, Ph.D. Thesis, Department of Mechanical and Aerospace Engineering, Case Western Reserve University, Cleveland, Ohio, expected October 1992.

2. T'ien, J. S., Combustion and Flame, 65, 1, pp. 31-34 (1986).

3. Olson, S. L Ferkul, P. V., and T'ien, J. S., 22nd Sym. (Int.) on Combustion, The Combustion Inst., pp. 1213-1222 (1988).

4. Grayson, G. D.: An Experimental Study of Low-Speed Concurrent Flow Flame Spread over a Thin Fuel, M.S. Thesis, Department of Mechanical and Aerospace Engineering, Case Western Reserve University, Cleveland, Ohio (1991).

5. Loh, H. T. and Fernandez-Pello, A. C.: Flow Assisted Flame Spread over Thermally Thin Fuels, proceedings of the First International Sym. on Fire Science, Hemisphere (1986).

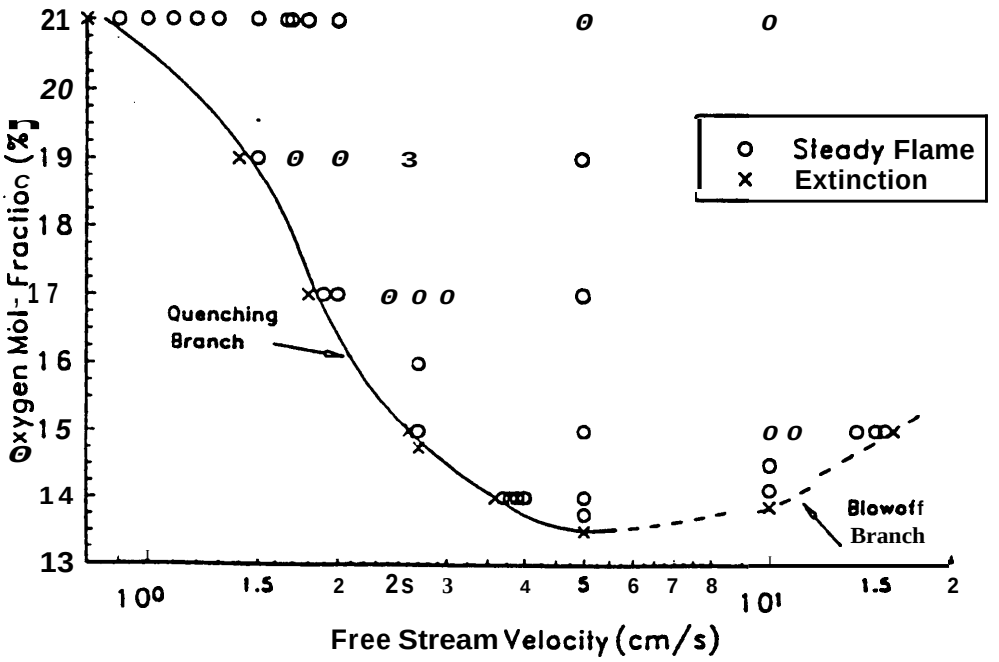

Fig. 1 Extinction Boundary of a Thin Solid Fuel in Concurrent Flow

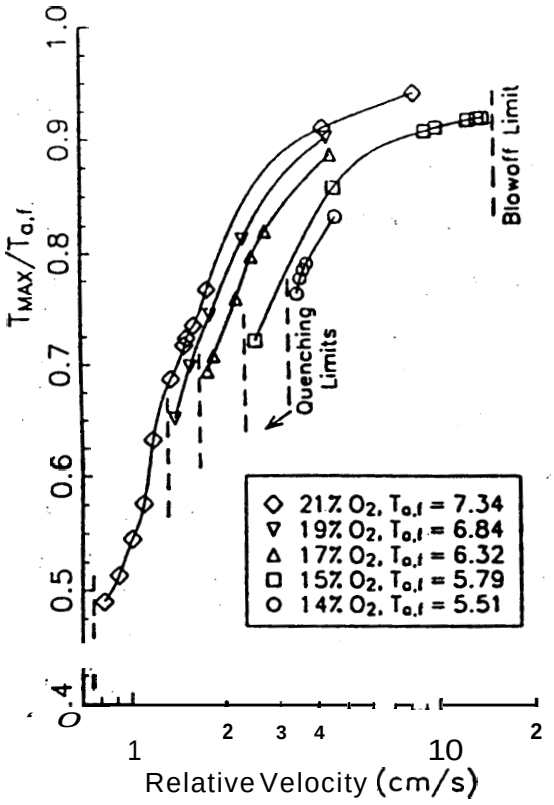

Fig. 2 Maximum Flame Temperature

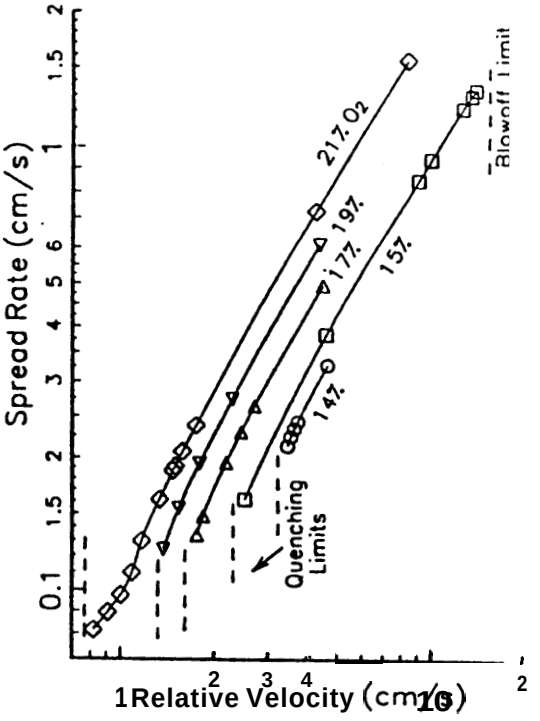

Fig. 3 Flame Spread Rate

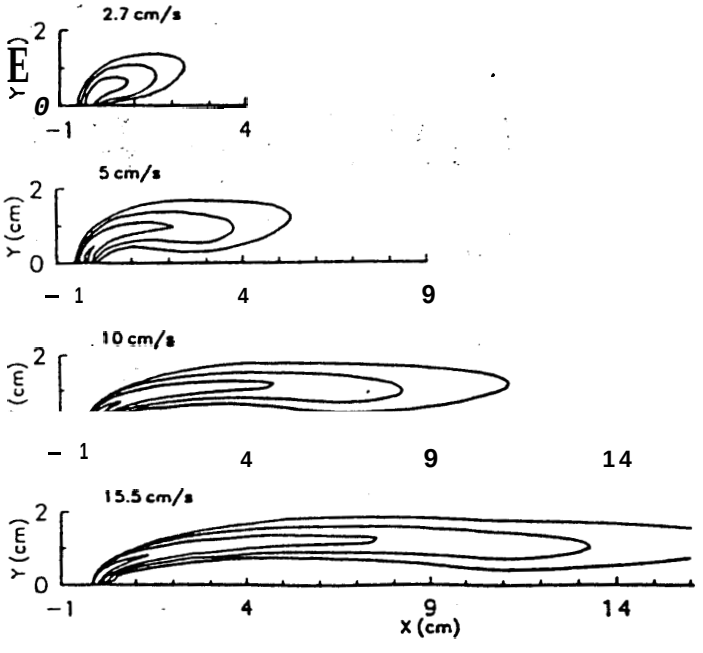

Fig. 4 Reactivity Contours at 15% Oxygen from Quenching to Blowoff (Outermost contour is 10^{-6} g/cm^3/s; a factor of 2 separates contours)

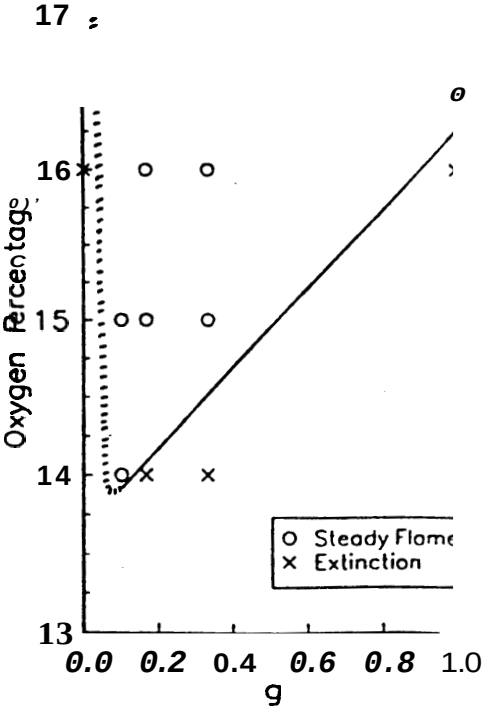

Fig. 5 Extinction Boundary for Kimwipe in Buoyant Opposed Flows (earth: g = 1)

TIEN, SACKSTEDER, FERKUL

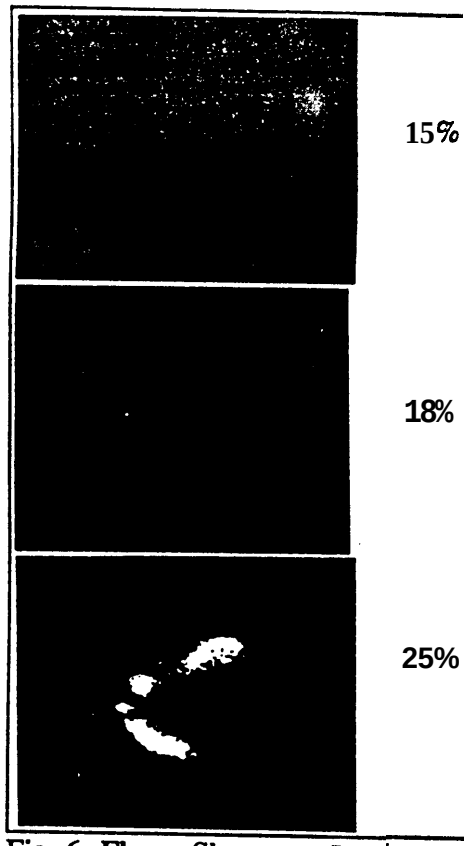

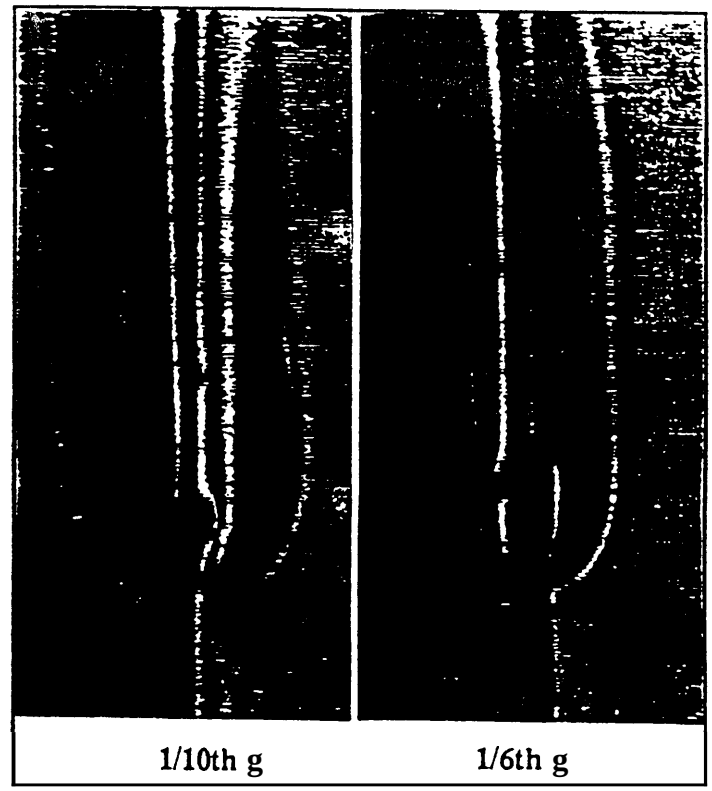

Fig. 6 Flame Shapes at 5cm/sec Relative Concurrent Flow

Fig. 8 Upward Spreading in 15% Oxygen, 1 atm (a,b), 0.5 atm (c,d)

2.B. REPLACED WITH COLOR PAGE

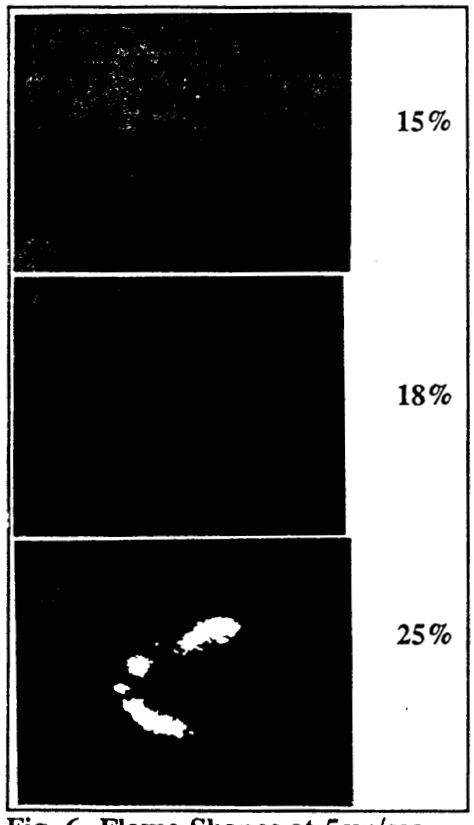

Fig. 6 Flame Shapes at 5cm/sec Relative Concurrent Flow

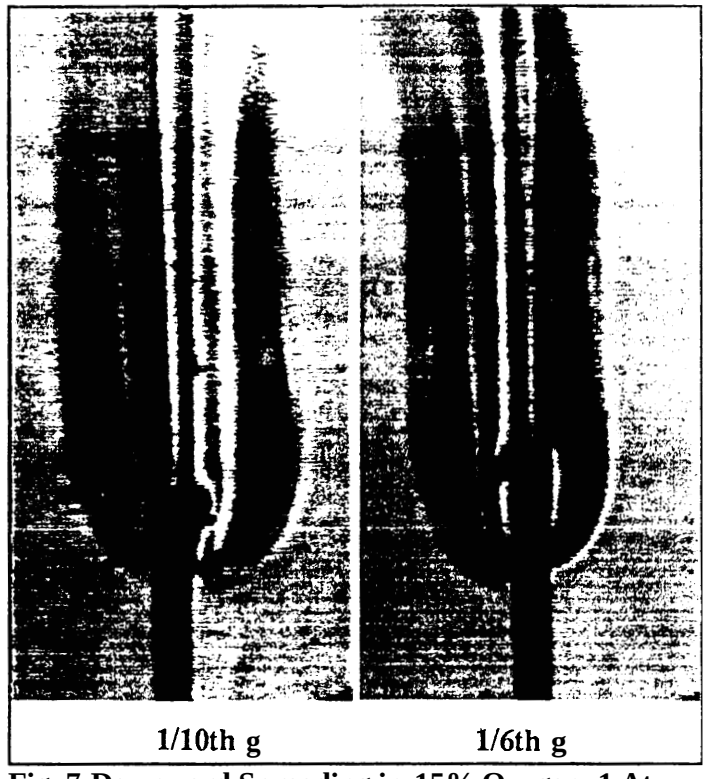

Fig. 7 Downward Spreading in 15% Oxygen, 1 Atm

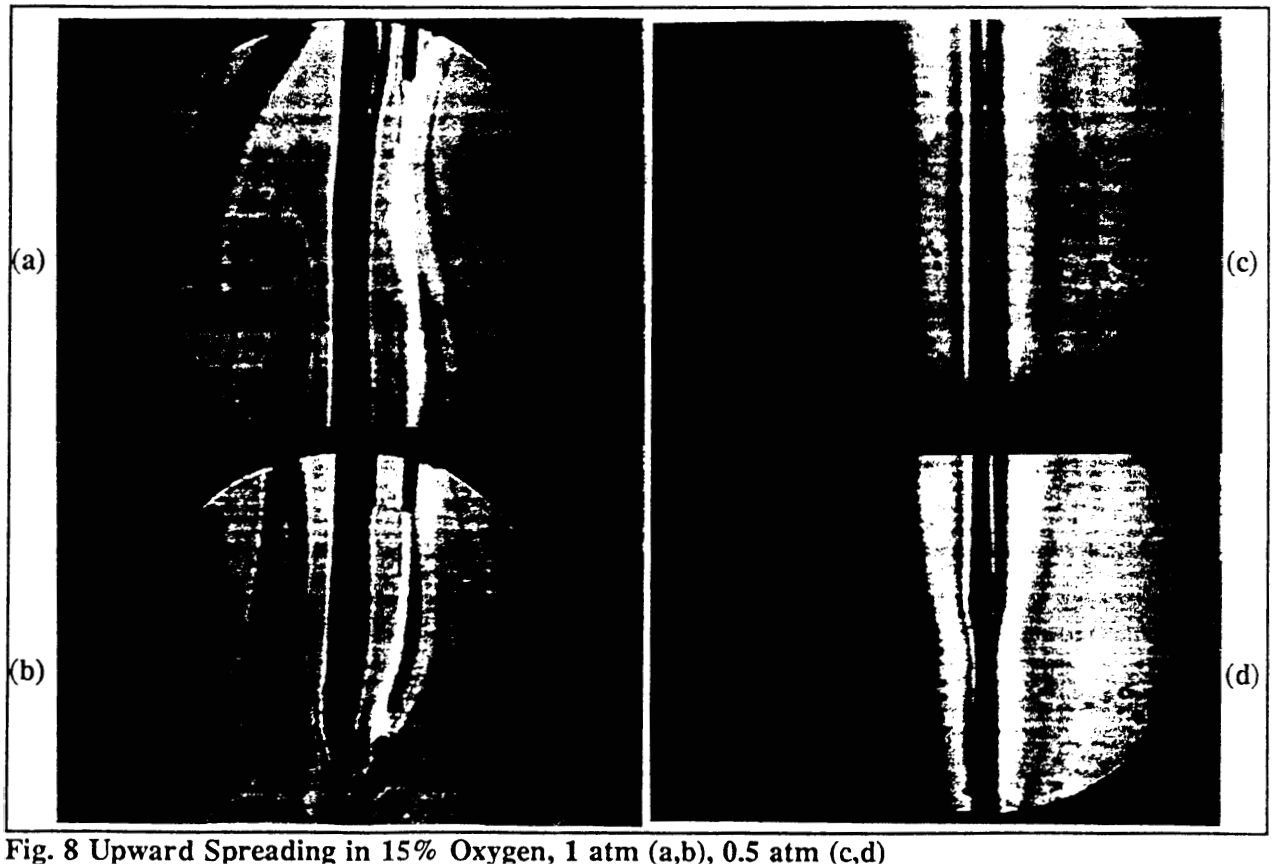

Fig. 8 Upward Spreading in 15% Oxygen, 1 atm (a,b), 0.5 atm (c,d)